The INAD Scaffold Is a Dynamic, Redox-Regulated Modulator of Signaling in the *Drosophila* Eye

Wei Liu,[1,6] Wenyu Wen,[3,4,6] Zhiyi Wei,[1,2] Jiang Yu,[1] Fei Ye,[1] Che-Hsiung Liu,[5] Roger C. Hardie,[5] and Mingjie Zhang[1,*]
[1]Division of Life Science, Molecular Neuroscience Center, State Key Laboratory of Molecular Neuroscience
[2]Institute of Advance Studies
Hong Kong University of Science and Technology, Clear Water Bay, Kowloon, Hong Kong
[3]Department of Chemistry
[4]Institute of Biomedical Sciences
Fudan University, Shanghai 200032, P.R. China
[5]Department of Physiology, Development, and Neuroscience, Cambridge University, Cambridge CB2 3DY, UK
[6]These authors contributed equally to this work
*Correspondence: mzhang@ust.hk
DOI 10.1016/j.cell.2011.05.015

SUMMARY

INAD is a scaffolding protein that regulates signaling in *Drosophila* photoreceptors. One of its PDZ domains, PDZ5, cycles between reduced and oxidized forms in response to light, but it is unclear how light affects its redox potential. Through biochemical and structural studies, we show that the redox potential of PDZ5 is allosterically regulated by its interaction with another INAD domain, PDZ4. Whereas isolated PDZ5 is stable in the oxidized state, formation of a PDZ45 ''supramodule'' locks PDZ5 in the reduced state by raising the redox potential of its Cys606/Cys645 disulfide bond by $\sim$330 mV. Acidification, potentially mediated via light and PLCβ-mediated hydrolysis of PIP$_2$, disrupts the interaction between PDZ4 and PDZ5, leading to PDZ5 oxidation and dissociation from the TRP Ca^{2+} channel, a key component of fly visual signaling. These results show that scaffolding proteins can actively modulate the intrinsic redox potentials of their disulfide bonds to exert regulatory roles in signaling.

INTRODUCTION

Scaffold proteins serve as platforms in signaling pathways by nucleating multiple proteins into macromolecular complexes and targeting them to specific regions within cells, and are critical for both efficiency and specificity of signaling events (Bhattacharyya et al., 2006; Pawson and Nash, 2003; Zhang and Wang, 2003). The *Drosophila* visual PDZ domain protein Inactivation, no after-potential D (INAD) is one of the best understood model systems for the roles of scaffolding in signal transduction (Huber, 2001; Montell, 1999; Tsunoda and Zuker, 1999). Within

the microvilli of fly photoreceptor cells, INAD organizes the core components of the phototransduction pathway into a supramolecular complex, involving the Ca^{2+}-permeable transient receptor potential (TRP) channel, phospholipase Cβ (PLCβ/ NORPA), and eye-specific protein kinase C (ePKC) via distinct PDZ domains, thus efficiently linking the G protein-coupled receptor rhodopsin to the Ca^{2+}-mediated signaling cascades (Adamski et al., 1998; Chevesich et al., 1997; Huber et al., 1996a; Kimple et al., 2001; Montell, 2005; Peng et al., 2008; Shieh and Zhu, 1996; Tsunoda et al., 1997; van Huizen et al., 1998; Wang and Montell, 2007). In this cascade, light photoisomerises rhodopsin, which activates PLCβ via the heterotrimeric Gq protein. PLCβ hydrolyses phosphatidylinositol 4,5-bisphosphate (PIP$_2$), releasing inositol 1,4,5-trisphosphate (IP$_3$) and 1,2-diacylglycerol (DAG) and a proton, which leads to opening of TRP channels, and depolarization of photoreceptor cells (Huang et al., 2010; for reviews, see Hardie and Raghu 2001; Wang and Montell 2007; Hardie and Postma 2008). DAG is also a potent activator of eye-PKC which phosphorylates both TRP and INAD and plays a key role in the termination of the light response (Popescu et al., 2006; Smith et al., 1991; Hardie et al., 1993; Gu et al., 2005; Huber et al., 1996b; Peng et al., 2008). Via the INAD-mediated assembly of the signaling complex, fly photoreceptors can respond to light with extremely fast kinetics (for reviews, see Tsunoda and Zuker 1999; Huber 2001; Hardie and Raghu 2001; Wang and Montell 2007; Hardie and Postma 2008) and adapt to a huge dynamic range of light intensities (Juusola and Hardie, 2001).

A recent study indicated that in addition to acting as a master scaffolding protein, INAD plays a critical dynamic role in regulating phototransduction on a millisecond timescale (Mishra et al., 2007). Namely, a pair of Cys residues in INAD PDZ5 (Cys606 and Cys645) undergo reversible, disulfide-mediated oxidation in response to light. When flies are kept in the dark, the two Cys residues in PDZ5 are in the reduced form. Upon exposure to bright light, PDZ5 is converted to the oxidized state by formation of the intramolecular Cys606-Cys645 disulfide

bond. Importantly, the authors demonstrated that this transient, light-dependent disulfide-mediated oxidation is required for efficient visual signal termination as well as visually mediated reflex behavior of flies (Mishra et al., 2007).

However, there are a number of major conceptual challenges regarding the mechanistic basis of the INAD-mediated dynamic signaling. Most critically, the redox potential surrounding the INAD-organized signaling complex microvilli is not expected to fluctuate with large amplitude on a millisecond timescale in response to light. This immediately begs the question: how is the light-dependent, transient disulfide bond formation/breaking of INAD PDZ5 achieved? Additionally, it was shown that the ePKC is required for the conformational switch of PDZ5 (Mishra et al., 2007). However, PDZ5 does not contain any obvious PKC phosphorylation sites. Furthermore, it is not clear how INAD PDZ5 maintains the reduced state when flies are kept in dark as the PDZ5 disulfide is highly stable due to its extremely negative redox potential. Finally, although the structure of INAD PDZ5 in its oxidized form contains a somewhat deformed target-binding groove (Mishra et al., 2007), it has not been proven that the target binding of INAD PDZ5 is disulfide bond dependent.

Here, we demonstrate that the redox potential of INAD PDZ5 is allosterically regulated by the direct conformational coupling of the fourth and fifth PDZ domains. Formation of the PDZ45 supramodule locks PDZ5 in the reduced state. Acidification uncouples the PDZ45 tandem and thereby unlocks its reduced conformation followed by the dissociation of the TRP channel from PDZ5. The allosteric regulation of the redox potential fluctuation of the INAD PDZ5 disulfide bond at a range of ~330 mV is unprecedented for cellular signaling proteins. This protein redox potential regulation mechanism may have general implications in other cell signaling processes that utilize disulfide bond containing intracellular proteins. Finally, regulation of protein conformational couplings by protons originating from PLC-mediated PIP_2 hydrolysis may represent a new paradigm for cellular signal transduction in general.

RESULTS

Identification of Specific INAD PDZ5 Ligands

The most plausible explanation for the INAD PDZ5 disulfide-mediated visual signal regulation is that the two PDZ5 conformers have distinct target-binding properties. Oxidation of PDZ5 may cause temporary dissociation of its target, and thereby terminate signaling. Although PDZ5 has been implied to interact with PLCβ (Tsunoda et al., 1997; van Huizen et al., 1998), the direct interaction between PDZ5/PLCβ remains controversial (Mishra et al., 2007; Xu et al., 1998), partly due to a sequencing error of PLCβ (the penultimate residue should be a "Tyr" instead of a "Cys" as originally reported). Identification of a specific PDZ5 target would be highly valuable in evaluating the mechanistic basis of the redox-dependent target binding of the domain. Aided by structure-based prediction of potential PDZ5 binders, we screened a small PDZ-binding peptide library. Among twelve peptides tested, the carboxyl peptide of proteoglycan NG2 showed the highest binding affinity toward reduced PDZ5 (Figure 1A). These data also demonstrated that a bulky
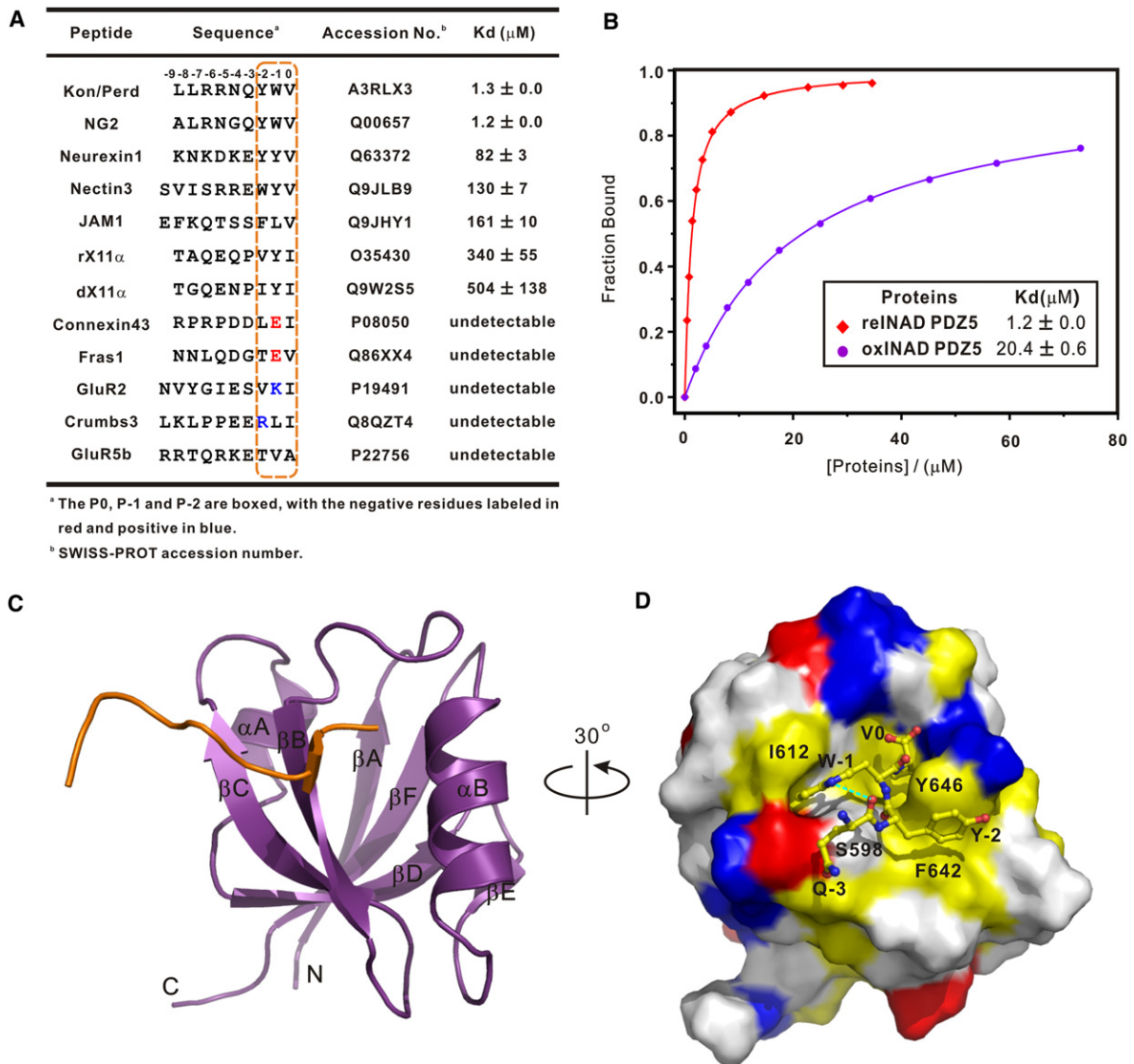
aromatic residue at the −2 position is critical, and Trp at the −1 position is highly preferred for carboxyl peptides to bind to PDZ5. The *Drosophila* ortholog of NG2 is Kon-tiki/Perdido (Kon/Perd), which has the same C-terminal four amino acids as NG2 (Figure 1A). As expected, the Kon peptide binds to PDZ5 with the same affinity as the NG2 peptide (Figure 1A). A search of the *Drosophila* genome for proteins containing the carboxyl tail peptide sequences of "YWΨ" ("Ψ" represents Val, Leu, and Ile) identified Kon/Perd as the only match. Although the physiological relevance, if any, of the INAD PDZ5/Kon interaction is unknown, identification of Kon as a high-affinity PDZ5 ligand provides a powerful tool for investigating the impact of the PDZ5 conformational switch on its target binding. We demonstrate that the reduced-to-oxidized conformational transition of PDZ5 induces a ~20-fold decrease in its affinity for the Kon peptide (Figure 1B; see Figures S1A–S1C available online), supporting the structure-based prediction that oxidation of PDZ5 can weaken its target binding (Mishra et al., 2007).

Solution Structure of the INAD PDZ5-Kon Tail Peptide Complex

To elucidate the molecular mechanism governing their specific interaction, we solved the solution structure of the reduced PDZ5/Kon peptide complex (Figure 1C; Figure S1D and Table S1). INAD PDZ5 adopts a canonical PDZ fold similar to its ligand-free form (Figure 1C) (Mishra et al., 2007). The Kon peptide binds to the αB/βB groove of INAD PDZ5 by pairing antiparallelly with βB. The side chain of Val(0) of the Kon peptide inserts into the hydrophobic pocket at the end of the αB/βB groove. The side chain of Trp(−1) makes extensive contacts with Ile612 from βC and Ser598 from βB of PDZ5. A hydrogen bond between the side-chain amide of Trp(−1) and the backbone carbonyl of Gln(−3) further stabilizes the bound peptide. The side chain of Tyr(−2) is sandwiched between the aromatic rings of Tyr646 and Phe642 from αB (Figure 1D). The complex structure explains the high selectivity of PDZ5 for the Trp(−1) and Tyr(−2) in the Kon peptide.

Isolated PDZ5 Cannot Spontaneously Cycle between the Reduced and Oxidized Conformers

In view of fast timescale of the fly visual signaling, we asked whether INAD PDZ5 might be able to cycle rapidly between the reduced and oxidized conformations by nuclear magnetic resonance (NMR) spectroscopy. The NMR spectrum of PDZ5 purified with buffer containing 1 mM DTT showed two distinct sets of peaks, each corresponding to the reduced and oxidized states (Figure S2A). The result indicates that 1 mM DTT cannot reduce PDZ5 and the coexisting reduced and oxidized conformers exchange at a slow NMR timescale. PDZ5 could be completely oxidized when the purified protein was passed through a preparative gel filtration column twice with the column buffer undegassed and free of reducing reagent (Figure 2A, top trace). Upon addition of 10 mM DTT, the oxidized PDZ underwent a time-dependent conversion to its reduced state (Figures 2A and 2B). The measured rate constant (from oxidized to reduced state) is ~0.3 $M^{-1} \cdot min^{-1}$, which is very slow considering the fast fly visual signaling events. We further measured the standard redox potential of the Cys606-Cys645 disulfide bond by

A

Peptide	Sequence[a]	Accession No.[b]	Kd (μM)
	-9-8-7-6-5-4-3-2-1 0		
Kon/Perd	LLRRNQ**YWV**	A3RLX3	1.3 ± 0.0
NG2	ALRNGQ**YWV**	Q00657	1.2 ± 0.0
Neurexin1	KNKDKE**YYV**	Q63372	82 ± 3
Nectin3	SVISRRE**WYV**	Q9JLB9	130 ± 7
JAM1	EFKQTSS**FLV**	Q9JHY1	161 ± 10
rX11α	TAQEQP**VYI**	O35430	340 ± 55
dX11α	TGQENP**IYI**	Q9W2S5	504 ± 138
Connexin43	RPRPDD**LEI**	P08050	undetectable
Fras1	NNLQDG**TEV**	Q86XX4	undetectable
GluR2	NVYGIES**VKI**	P19491	undetectable
Crumbs3	LKLPPEE**RLI**	Q8QZT4	undetectable
GluR5b	RRTQRKE**TVA**	P22756	undetectable

[a] The P0, P-1 and P-2 are boxed, with the negative residues labeled in red and positive in blue.

[b] SWISS-PROT accession number.

B

Proteins	Kd(μM)
◆ reINAD PDZ5	1.2 ± 0.0
● oxINAD PDZ5	20.4 ± 0.6

C

D

Figure 1. Discovery of Specific Binding Targets of INAD PDZ5

(A) Summary of the screening results for the reduced PDZ5-binding peptides. The binding affinities were derived from fluorescence polarization titration-based measurements.

(B) Fluorescence polarization titration-derived binding affinities of reduced and oxidized PDZ5 to the Kon peptide.

(C) Ribbon diagram of a representative NMR structure of the PDZ5/Kon peptide complex. The PDZ5 is shown in purple, and the Kon peptide in orange.

(D) The combined surface (PDZ5) and stick (the Kon peptide) models showing the interaction between PDZ5 and the Kon peptide. The positively charged amino acids of PDZ5 are highlighted in blue, the negatively charged residues in red, the hydrophobic residues in yellow, and the others in white.

Also see Figure S1.

NMR spectroscopy using DTT as the redox potential buffer (Figure 2C). The conversion reaction at each DTT concentration was considered to be in equilibrium if the peak intensities of two spectra acquired for the same mixture were the same after 5 hr. The measured standard redox potential for the Cys606-Cys645 disulfide formation is −0.37 V (Figure 2D), a value far below the standard redox potentials of the cytoplasmic milieu in most cells (−0.2∼−0.3 V) (Keese et al., 1999; Ostergaard et al., 2004; Schafer and Buettner, 2001). Thus, both kinetic and thermodynamic data indicate that INAD PDZ5 is highly stable in its oxidized form and cannot spontaneously cycle between the reduced and oxidized conformations at speeds compatible with visual signaling. This implies that other factors must interact directly or indirectly with PDZ5 to regulate its redox potential and redox-dependent conformational cycling.

PDZ4&5 Interact with Each Other to Form a Supramodule

Tandem PDZ repeats often display distinct structural and functional properties when compared with individual PDZ domains
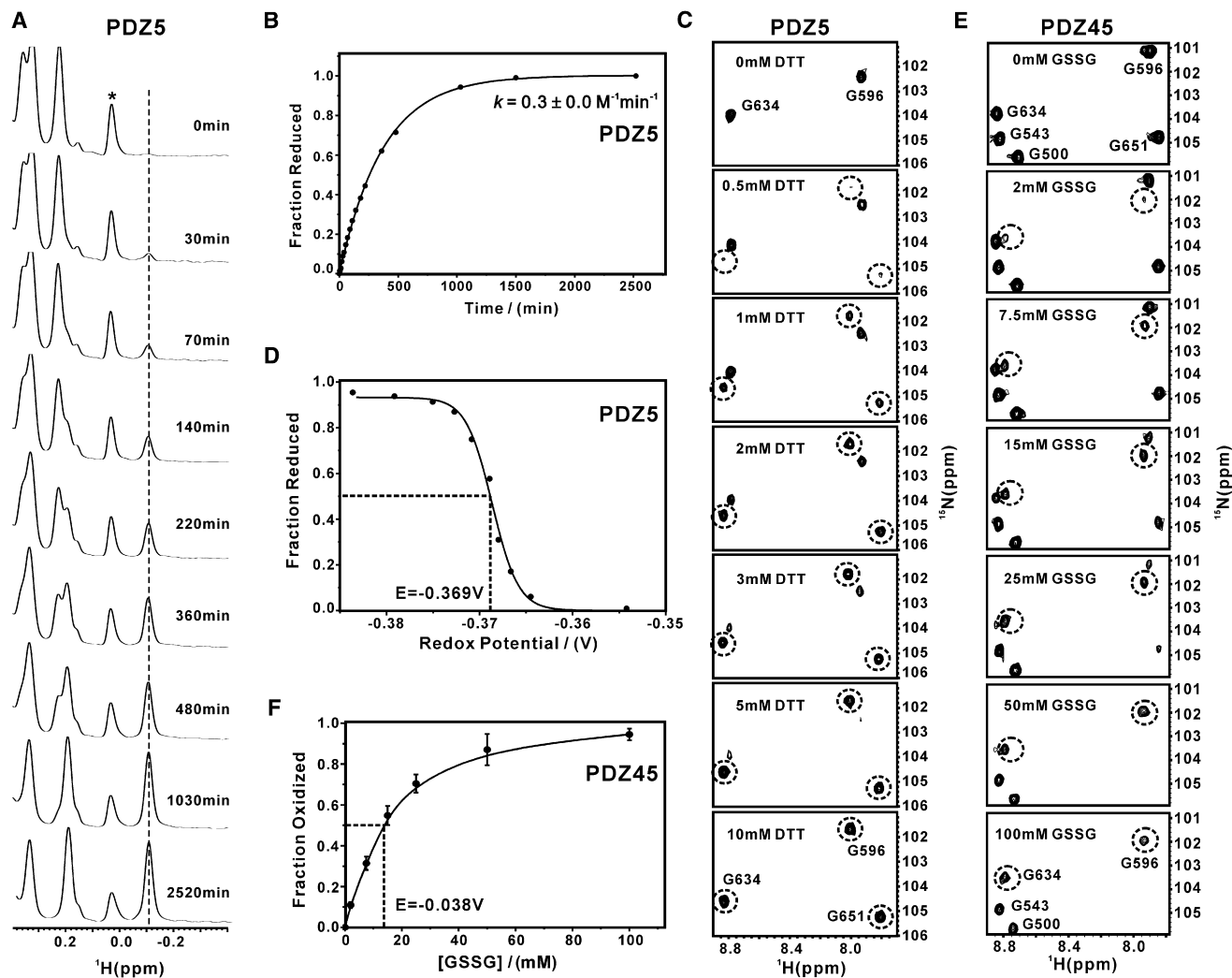
Figure 2. The Oxidation Kinetics and the Redox Potential of the Isolated PDZ5 and the PDZ45 Tandem

(A) Oxidized PDZ5 (0.5 mM) was mixed with 10 mM reduced DTT, a selected methyl region of the ^{1}H-NMR spectrum was recorded as a function of time. The methyl peak at −0.11 ppm was used for deriving the reduction rate constant of PDZ5. The peak indicated with asterisk was a volatile contaminant.

(B) Second-order reduction kinetics curve derived from (A).

(C) Selected regions of ^{1}H, ^{15}N HSQC spectra of PDZ5 showing the equilibrium of the reduced and oxidized forms of PDZ5 during the DTT titration. The peaks corresponding to the newly appeared, reduced form of PDZ5 are highlighted with dotted circles.

(D) The standard redox potential of PDZ5 was determined by fitting the curve of the fraction of reduced protein as a function of the redox potential of the sample buffer at each titration point.

(E) Selected regions of ^{1}H, ^{15}N HSQC spectra of PDZ45 showing the equilibrium of the reduced and oxidized forms of PDZ45 during the GSSG titration. The peaks corresponding to the oxidized form of PDZ5 are highlighted with dotted circles.

(F) By fitting the curve of the fraction of oxidized protein as a function of the GSSG concentration, the standard redox potential of PDZ5 in PDZ45 was determined as the redox potential of the sample buffer at the 50% of PDZ45 oxidation. The fraction of oxidized PDZ45 at each GSSG concentration was derived by averaging the peak intensities ratios (I_{ox}/I_{ox+re}) of multiple well-resolved peaks in the HSQC spectrum upon the oxidation reaction reached to equilibrium.

Also see Figure S2.

(Feng et al., 2003; Feng and Zhang, 2009; Long et al., 2005). Because the INAD PDZ4 and PDZ5 domains are connected by a short linker with only 5 residues, we hypothesized that the PDZ45 tandem of INAD may also form a supramodule. Extensive trials of the domain boundaries showed that inclusions of a 10 residue extension N-terminal to PDZ4 and the entire C-terminal tail outside PDZ5 (i.e., residues 473–674, referred to as PDZ45

hereafter for simplicity) is essential for obtaining stable PDZ45 tandem samples. Different from the isolated PDZ5, the ^{1}H,^{15}N-HSQC NMR spectrum of PDZ45 purified with buffer containing 1 mM DTT showed only one set of well-dispersed peaks, corresponding to the fully reduced state (Figure S3A). Comparison of the HSQC spectra of PDZ45 and PDZ5, both in their reduced states, revealed significant chemical shift
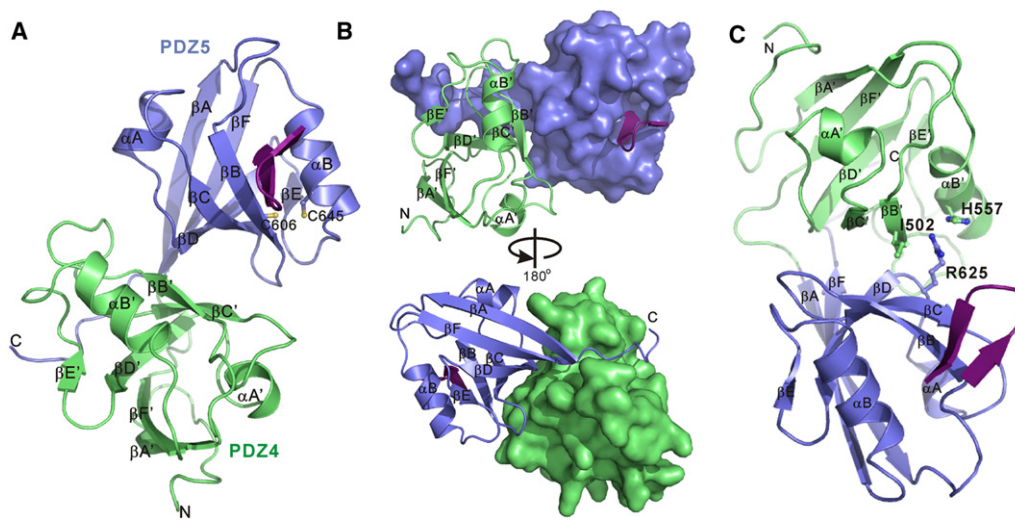
Figure 3. Crystal Structure of the PDZ45/NG2 Peptide Complex
(A) Ribbon diagram of the PDZ45/NG2 peptide complex with PDZ4 colored in green, PDZ5 in blue, and the NG2 peptide in magenta. Cys606 and Cys645 are highlighted in stick model.
(B) Combined ribbon and surface presentations showing the interdomain interaction in the PDZ45 tandem.
(C) Combined ribbon and stick models showing that the ligand-binding site of PDZ4 (the αB′/βB′ groove) is occluded by the side chain of Arg625 from PDZ5. Also see Figure S3 and Figure S4.

differences of PDZ5 between its isolated and its PDZ45 tandem forms (Figure S3A), indicating that PDZ4 and/or the extensions in the two termini interact with PDZ5. We mapped the chemical shift differences of PDZ5 between the two forms onto its structure (Figure S3B). Residues at the beginning of βA and end of βF of PDZ5 showed large chemical shift differences, and such shift changes are expected as these two regions are covalently connected to PDZ4 and the C-terminal extension, respectively, in PDZ45. Importantly, large chemical shift changes were observed for the residues in βB, βC (including Cys606 in the βC1 position), αB (including Cys645 in αB), as well as the rest of the target peptide-binding region of PDZ5 (Figure S3B), indicating that the interaction of PDZ4 has a long-range conformational impact on PDZ5. This finding immediately points to the possibility that the light-dependent formation of the disulfide bond in PDZ5 may be allosterically regulated by PDZ4 coupling.

Crystal Structure of the PDZ45/NG2 Complex
The excellent NMR spectrum of PDZ45 indicates that the protein adopts a monodispersed conformation favorable for crystallization. The structure of the PDZ45/NG2 peptide complex was solved using the single-wavelength anomalous dispersion method with Se-Met derivative and refined to 2.6 Å resolution (Table S2). Consistent with the NMR shift perturbation assay (Figure S3B), the two PDZ domains in PDZ45 physically interact with each other (Figure 3A). The interface between the two PDZ domains involves βB′, βC′, αB′, the βB′/βC′ loop, and the αA′/βD′ loop from PDZ4; and βB, βC, βD, the βB/βC loop, and the αA/βD loop from PDZ5 (Figure 3). Importantly, the C-terminal extension of PDZ5 (residues 664–674) tucks into a groove at the rear (relative to the putative target-binding groove) of PDZ4, physically stapling the two PDZ domains together (Figure 3B), revealing that the C terminus is essential

for the structural integrity of PDZ45. The N-terminal extension of PDZ4 interacts intimately with residues from βA′ and αA′, explaining why this extension is also necessary for obtaining the properly folded tandem.

Consistent with the Ellman assay result, PDZ5 in the PDZ45/NG2 peptide complex is in the reduced form (Figure 3A). The potential target-binding pocket of PDZ4 is occluded by the αA/βD loop of PDZ5 with the side chain of Arg625 inserting into the αB′/βB′ groove of PDZ4 (Figure 3C). The NG2 peptide binds to PDZ5 in a β-hairpin conformation (Figure 3A). The last 4 residues of the NG2 peptide bind to PDZ5 in the PDZ45 tandem in an identical manner to the Kon peptide binding to the isolated PDZ5 (Figure S3C). The main difference between the conformations of the target peptides in the NMR-derived PDZ5/Kon peptide complex and the X-ray-derived PDZ45/NG2 peptide complex is the lack of the mini-β strand of the PDZ5-bound Kon peptide (corresponding to Leu_{-8}-Leu_{-7}-Arg_{-6} of the Kon peptide, Figure 1), and this difference is likely to be an artifact of crystal packing (Figures S3C and S3D).

Formation of the PDZ45 Supramodule Dramatically Raises the Redox Potential of PDZ5
The direct interaction between PDZ4&5, together with the PDZ4 coupling-induced long-range conformational impact on PDZ5 revealed by NMR, hints that formation of the PDZ45 supramodule may alter the redox potential of PDZ5. To evaluate this possibility, we compared air-mediated oxidation of PDZ5 in its isolated and in the PDZ45 tandem forms. Reduced PDZ45 could not be oxidized after two or three cycles of gel-filtration chromatography (Figure 4A). Specifically, we can directly observe that the chemical shifts of Cys606 and Cys645 did not change at all from its reduced conformation during the entire process (highlighted in a green circle in Figure 4A). In addition to Cys645
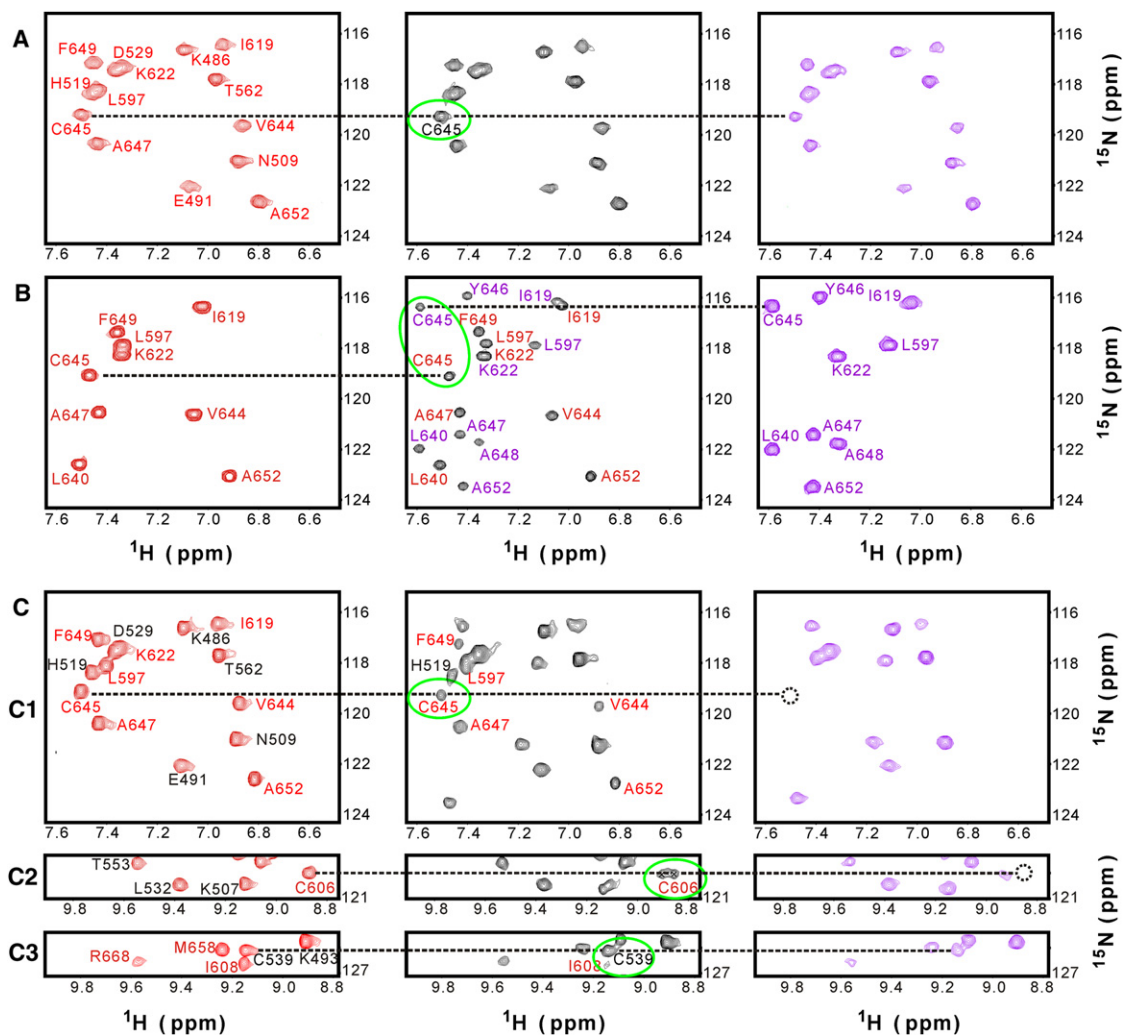
Figure 4. Formation of the PDZ45 Tandem Prevents the Disulfide-Mediated Oxidation of PDZ5

(A and B) Selected regions of ^{1}H, ^{15}N HSQC spectra of PDZ45 (A) and PDZ5 (B) during air oxygen-mediated oxidations of the proteins. In this experiment, ^{15}N-labeled PDZ45 (0.2 mM) was purified with 1 mM DTT, and PDZ5 (0.4 mM) was initially fully reduced by incubation with 10 mM DTT (left panels, red peaks). After rapid removal of DTT, each sample was passed through one (middle panel, black peaks) or two (right panels, magenta peaks) cycles of size-exclusion chromatography (Hiload 26/60 Superdex 200). The redox status of Cys645 in PDZ45 and PDZ5 are highlighted by green ovals. The dashed lines are used to highlight that Cys645 in the isolated PDZ5 is easily oxidized (with two distinct peaks in the middle panel), and the same Cys in PDZ45 is highly resistant to the oxidation.

(C) Selected regions of ^{1}H, ^{15}N HSQC spectra of PDZ45 during the GSSG-mediated oxidation at pH 7.0. In this experiment, ^{15}N-labeled fully reduced PDZ45 (0.2 mM) was incubated with 50 mM GSSG for 250 min (middle panel, black peaks) or 500 min (right panels, magenta peaks). The oxidation statuses of Cys606, Cys645, and Cys539 are highlighted by green ovals in C1, C2, and C3, respectively. For clarity, peaks from PDZ4 and PDZ5 are labeled in black and red, respectively.

Also see Figure S2, Figure S3, and Figure S4.

and Cys606 in PDZ5, the other three Cys residues in PDZ4 also remained in the reduced form (data not shown). We repeated the same experiment with reduced PDZ5, keeping the concentration of PDZ5 at about double of the PDZ45 to ensure that the total Cys concentrations in the two series of experiments were comparable. In sharp contrast to what was observed for PDZ45, the NMR spectrum of PDZ5 after passing one cycle of the gel filtration column showed that the protein is a mixture of reduced and oxidized forms with a roughly equal population (Figure 4B, middle panel). Another cycle of the column fully converted the protein into its oxidized form (Figure 4B, right panel). The results shown in Figures 4A and 4B indicate that coupling of PDZ4 allosterically alters the local environment of the Cys606&645 pair in PDZ5 and renders them more resistant to oxidation. As the overall conformation of the Cys606&645-harboring αB/βB groove remains largely the same upon forming the PDZ45 supramodule (Figure 1C and Figure 3), the decreased oxygen-mediated oxidation speed of PDZ5 in the PDZ45 tandem

likely correlates with an increased redox potential of the Cys606&645 pair in PDZ45.

To test the above hypothesis, we measured the standard redox potential of the Cys606-Cys645 disulfide in PDZ45. Because the reduced PDZ45 is highly stable even in sample buffers lacking any reducing reagents such as DTT, we performed PDZ45 oxidation experiment by incubating the protein in 50 mM Tris pH 7.0 containing increasing concentrations of GSSG. The oxidation of PDZ45 was monitored both by the Ellman assay and by NMR spectroscopy. The Ellman assay showed that only ~40% of total Cys residues (equivalent to two of five Cys) were oxidized when the oxidation reaction reached to an equilibrium state (Figure S2B). To assign which Cys residues were oxidized, we performed a series of time-dependent oxidation reactions of ^{15}N-labeled PDZ45 with increasing concentrations of GSSG. As shown in Figure 4C, GSSG-mediated oxidation of PDZ45 induced chemical shift changes to Cys645 (Figure 4C1) and Cys606 (Figure 4C2). Additionally, a number of other residues from PDZ5 (e.g., Gly596, Leu597, Phe649, Gly651, Ala652), which reside in close vicinity of the PDZ5 αB/βB groove and thus spatially close to Cys606&645, also showed obvious oxidation-induced chemical shift changes. In contrast the three Cys residues in PDZ4 (e.g., Cys539 shown in Figure 4C3) did not show detectable chemical shift changes upon PDZ45 oxidation. Taken together, the Ellman assay and NMR studies indicated that incubation of PDZ45 in the GSSG-containing buffer led to specific oxidation of the Cys606&645 pair in the PDZ45 tandem, and the remaining three Cys residues in PDZ4 were not oxidized.

The oxidation of PDZ45 by GSSG reached a steady/equilibrium state at ~7 hr after the initiation of the reaction (Figure S2C). By plotting the fraction of oxidized Cys606-Cys645 in PDZ45 at each equilibrium state as the function of the GSSG concentrations, we were able to measure the redox potential of the Cys606&645 pair in PDZ45, and the value is −0.038 V (Figure 2F). A very similar value (~−0.040 V) was obtained from the Ellman-based assays (Figure S2B). Taken together, our data unequivocally demonstrate that the formation of the PDZ45 supramodule stabilizes the reduced conformation of PDZ5 by dramatically raising the redox potential of the Cys606&645 pair. It is envisioned that the reduced Cys606 and Cys645 of PDZ45 is highly stable at the intracellular milieu with typical redox potentials of −0.2~−0.3 V. This is in stark contrast to the isolated PDZ5, of which the oxidized state is highly stable at the same cellular redox potentials (Figure 2). The standard redox potentials of PDZ5 in its isolated and in the PDZ45 tandem forms suggest that PDZ5 cannot spontaneously cycle between reduced and oxidized forms at the cellular milieu. We also noted that the Cys residues in PDZ45 have a much slower oxidation reaction speed than those in PDZ5 (Figures S2C and S2D). Therefore, it seems that additional factor(s) must function together with cellular oxidant(s) to oxidize the Cys606&645 pair of PDZ5.

Acidification Uncouples the PDZ45 Supramodule and Regulates the Conformational Cycling of PDZ5
Although PDZ4 modulates the redox potential of PDZ5 allosterically, the formation of the PDZ45 supramodule per se does not affect the target-binding property of PDZ5 (Figure 1B; Figure S4A). We investigated the allosteric conformational coupling between PDZ4&5 in response to the Kon peptide binding using NMR spectroscopy (Figures S4B and S4C). In line with the crystal structure, the Kon peptide specifically binds to PDZ5 (e.g., the large shift changes of Gly596 from the "GLGF" loop of PDZ5), but not to PDZ4 (e.g., no shift change of Gly500 from the "GLGF" loop of PDZ4). Importantly, in addition to residues directly involved in the binding of the Kon peptide, amino acid residues in the interface of PDZ4&5 also experienced substantial target peptide-induced chemical shift changes. This result, together with the data shown in Figure 4, reveals that the redox potential and the target binding of PDZ5 can be allosterically modulated by amino acid residues outside the domain.

We then tried to identify a potential regulatory switch for the redox potential cycling of PDZ5. The most obvious candidate was ePKC, as it is required for the light-induced oxidation of PDZ5 (Mishra et al., 2007), and PKC has been shown to phosphorylate INAD (Huber et al., 1996b; Popescu et al., 2006). PDZ45 contains two consensus PKC phosphorylation sites: Thr553 in αB of PDZ4 and Thr666 in the C-terminal tail of the tandem (Figure 5A). The two Thr residues play active roles in the packing of the C-terminal tail with PDZ4 and are therefore necessary for the formation of the PDZ45 supramodule (Figure S4D). Structural analysis predicts that phosphorylation of Thr553 and/or Thr666 would destabilize the interdomain interaction between PDZ4 and PDZ5 and thereby weaken or eliminate the allosteric coupling of the two PDZ domains. If this prediction is correct, the conformational cycling of PDZ5 could be explained by PKC-mediated phosphorylation of PDZ45.

To test this hypothesis, we made single and double Thr553Glu, Thr666Glu mutations to mimic PKC-mediated phosphorylation of PDZ45. Indeed, the Thr553,666Glu double mutant of PDZ45 led to enhanced oxidation in the H$_2$O$_2$-mediated oxidation assay (Figure S4E). However, to our disappointment, no obvious phosphorylations on Thr553/Thr666 (or on any other Thr and Ser residues in PDZ45) by PKC could be observed under numerous conditions tested (see Figures S5A–S5C for details).

We were forced to widen our screening by testing other Ser and Thr residues, which may function as the regulatory switch for the PDZ5 conformational cycling. Among many residues tested, we observed with extreme interest that substitution of Thr669 with Ala, a mutation originally designed to mimic non-phosphorylated state of the residue, led to dramatically increased phosphorylation of PDZ45 by PKC (Figure 5B). The level of PKC-mediated phosphorylation of T669A-PDZ45 is even higher than the phosphorylation of INAD PDZ2 that can be physically docked on to the kinase (the first lane, Figure 5B). Structural analysis of PDZ45 reveals that the side chain of Thr669 from the C-terminal tail forms a strong hydrogen bond with the imidazole ring of His547 in PDZ4 (the average bond length of ~2.7 Å in the eight PDZ45 molecules in each asymmetric crystal unit; Figure 5D). Substitution of Thr669 with Ala would eliminate the Thr669-His547 H-bond and thereby lead to uncoupling of the PDZ45 supramodule. Indeed, the T669A mutation of PDZ45 can be rapidly oxidized by a low concentration of H$_2$O$_2$ (88 μM) at pH 7.5 when compared with the WT PDZ45 (Figure 5C). It was shown recently by one of us (R.C.H.) that fly microvilli undergo
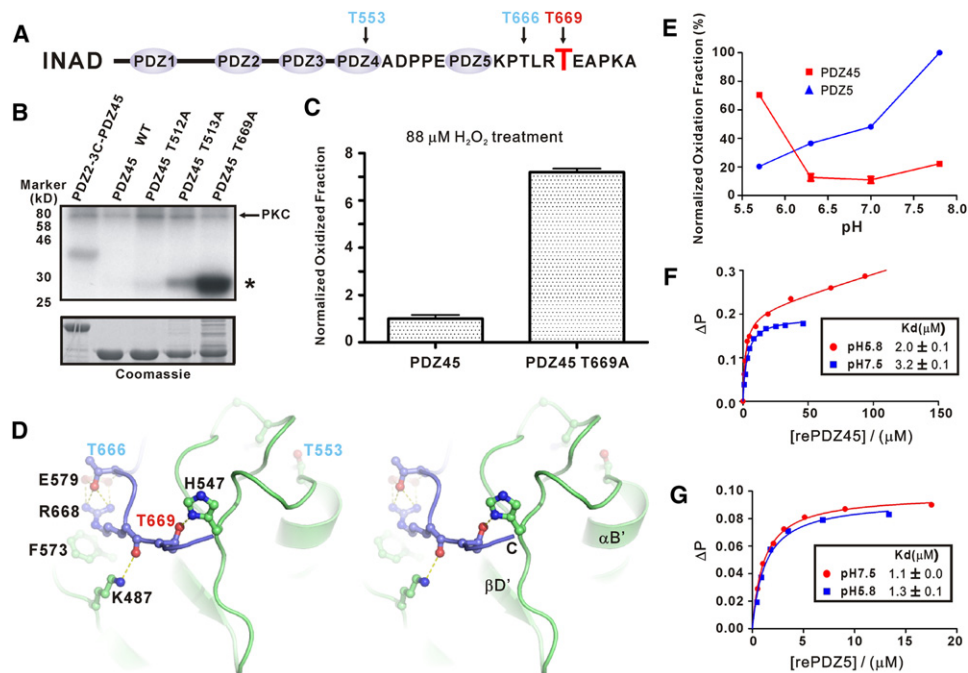
Figure 5. pH-Regulated, Allosteric Regulation of the PDZ45 Redox Potential

(A) The domain organization of INAD showing the two predicted PKC phosphorylation sites (Thr553 and Thr666), as well as Thr669 in PDZ45.

(B) Substitution of Thr669 with Ala of PDZ45 led to its massive phosphorylation by PKC. Substitution of Thr513 in the PDZ45 interface also led to an increase of its phosphorylation. No detectable PKC-mediated phosphorylation occurred for WT PDZ45. The weak phosphorylation of "PDZ2-3C-PDZ45" is from the PDZ2, as all phosphorylation signals originate from the PDZ2 part (see Figure S5B).

(C) The T669A-PDZ45 is much more susceptible to oxidation at pH 7.5. The figure shows that the mutant can be easily oxidized by a low concentration of H_2O_2. Error bars show mean ± standard deviation (SD) for three different experiments.

(D) Stereoview showing a strong hydrogen bond formed by the hydroxyl group of Thr669 and the imidazol ring of His547. The figure also shows the H-bond network formed between Thr666 with its neighboring residues, and these interactions would be stabilized by the Thr669-His547 H-bond.

(E) Comparison of the pH dependent oxidations of PDZ5 (75 μM) and PDZ45 (30 μM) in the presence of 5 mM GSSG.

(F and G) Fluorescence polarization assays showing that both PDZ45 (F) and PDZ5 (G), in their reduced forms, display similar Kon peptide-binding affinities at pH 7.5 and 5.8.

Also see Figure S5.

rapid, light-induced acidification due to protons released by PLCβ-mediated hydrolysis of PIP$_2$ (Huang et al., 2010). It was shown that light activation leads to 0.1–0.2 pH unit change to the entire cell body and this pH change originates from rhabdomere. Although direct measurements of the local pH change are not available, a simple calculation taking account of the space occupied by the INAD-organized signaling complex and the volume of the entire rhabdomere, suggests that light-induced release of protons in the immediate vicinity of the INAD-organized signaling complex could lead to a decrease of several pH units. Such a pH decrease is capable of breaking the Thr669/His547 H-bond due to the protonation of His547 imidazole ring. In other words, protons produced by the light-induced PLC activity may act as the regulatory switch for the conformational coupling of the PDZ45 supramodule.

Several lines of experimental evidence support the pH-induced conformational cycling model of PDZ45. First, CD and NMR experiments showed that PDZ45 displays a pH-dependent conformational change with major spectral changes occurring at pH ~6.0, a value matching pKa of a His side chain (Figures S5D–S5I). Second, one would predict that the redox potential

of PDZ5 in the PDZ45 tandem would undergo a sudden drop upon protonation of His547. Indeed, GSSG-mediated oxidation of PDZ45 displayed a pH-dependent decrease when pH of the sample buffer was lowered from 7.8 to 6.3, which is due to increased protonation of Cys606 and Cys645 at more acidic conditions (Figure 5E). The GSSG-mediated oxidation of Cys606 and Cys645 in PDZ45 showed a sudden surge when pH of the buffer was further lowered from 6.3 to 5.8 (Figure 5E), presumably due to the His547 protonation-induced uncoupling of PDZ4&5. In comparison, the GSSG-mediated oxidation of PDZ5 alone followed a predicted pH-dependent decrease upon lowering the buffer pH (Figure 5E). Third, the oxidation speed (mediated by either GSSG or H_2O_2) of PDZ45 was dramatically enhanced when pH of the sample buffer dropped from neutral condition to pH 5.8 (Figures S5J and S5K). We noticed that that PDZ5 in the PDZ45 tandem is even more susceptible to oxidation than the isolated PDZ5 at acidic pH conditions, possibly due to a new mode of interaction between PDZ4 and PDZ5 at low pH conditions (Figure 5E; Figure S5K). Importantly, the decrease of pH does not induce overall unfolding of PDZ5 in the PDZ45 tandem (Figure S5D), and PDZ5 or PDZ45 in the

reduced form binds to target peptides with comparable affinities at pH 7.5 or 5.8 (Figures 5F and 5G).

INAD Binds to Two Discrete Sites of the TRP Channel Using Its PDZ3 and PDZ45 Domains

The identification of the Kon peptide as a specific binder of PDZ5 prompted us to search for other potential PDZ5 targets in the *Drosophila* proteome. Interestingly, one candidate identified was the TRP channel (Figure 6A). We tested the binding between the C-terminal "GWL" motif of the TRP channel with INAD using a synthetic peptide containing the last 9 residues of TRP ("TGRMISGWL") and found that this TRP peptide binds to PDZ45 with a low affinity (Kd ~140 μM, Figure 6B). NMR-based assays revealed that the peptide binds to the same pocket as the Kon peptide does (Figure 6C), indicating that the weak interaction between the TRP tail and PDZ45 is specific. In vivo, TRP forms multimers (Montell, 2003) and INAD also has a tendency to form oligomers (Xu et al., 1998). The multimerizations of both TRP and INAD could increase the binding avidity of the two proteins.

It has been shown that an internal sequence (the "^{1264}STV^{1266}" motif, Figure 6A) of TRP is also required for TRP to interact with INAD, most likely via binding to PDZ3 (Li and Montell, 2000; Peng et al., 2008). We confirmed this finding using a GST-fused TRP peptide contain both the "^{1264}STV^{1266}" and the "GWL" motifs. The WT GST-fused TRP peptide robustly binds to the purified full-length INAD (Figure 6D). Substitution of Val1266 with Ala weakens its interaction with INAD, and the replacement of Trp1274 with Ala eliminated the binding (Figure 6D). In contrast, the GST-fused TRP peptides showed no detectable binding to PDZ45 due to very weak interaction between the "GWL" motif of TRP and PDZ5 of INAD (Figure 6E).

We were able to purify a highly stable PDZ345/TRP C-terminal tail complex by coexpressing INAD PDZ345 and GB1-tagged TRPCT containing the last 15 residues (GB1-TRPCT) (Figure 6F). The INAD/TRP complex has a Kd of ~0.1 μM (Figure S6A), further confirming the stable bidentate interaction between PDZ345 and the TRPCT. If PIP$_2$ hydrolysis induced acidification indeed functions as a regulatory switch of the Cys606&645 oxidation, one would predict that the PDZ345/TPRCT complex would be stable at neutral pH. Lowering pH of the PDZ345/TPRCT complex sample would promote dissociation of the complex under oxidation conditions due to the protonation of His547. Exactly as predicted, the PDZ345/TRPCT complex remains stable even when the sample was treated with H$_2$O$_2$ (Figure 6F). In contrast, at low pH, even without H$_2$O$_2$, partial GB1-TRPCT dissociation from PDZ345 could be detected. We suspect that this pH-induced, partial PDZ345/TRPCT dissociation may result from the uncoupling of PDZ3 from PDZ45. Treatment of the PDZ345/TRPCT complex at pH 5.8 with H$_2$O$_2$ further promoted the complex dissociation (Figure 6F).

The data in Figures 6B–6F and the results from earlier studies (Li and Montell, 2000; Peng et al., 2008) together reveal that the TRP channel uses two discrete binding sites to bind to PDZ3 and PDZ5 of INAD. Such a bidentate interaction between TRP and INAD would afford tight TRP/INAD complex formation, even though each site alone has relatively weak affinity. The multimerization-induced avidity effect would further enhance the TRP/

INAD complex formation. More importantly, the bidentate interaction between TRP and INAD has a regulatory advantage in controlling the assembly between TRP and INAD, as the complex can be efficiently dissociated by disrupting either one of the two binding sites (e.g., via PDZ5 oxidation, Figure 7H). Reciprocally, the multimerization property of TRP channel would further promote the disassembling of the TRP/INAD complex, thus generating a sharp transition between the complexed and the uncomplexed states.

Interestingly, although isolated PDZ5 has no detectable binding to the C-terminal tail of PLCβ, the PDZ45 tandem binds to the PLCβ tail peptide with a Kd ~30 μM (Figures S6B and S6C). This finding is consistent with an earlier report showing that a mutation in PDZ5 of INAD (*inaD^2*) leads to dissociation of PLCβ from INAD (Tsunoda et al., 1997). Importantly, GSSG-mediated oxidation of PDZ45 abolished the tandem's PLCβ tail peptide binding (Figure S6C), pointing to a possibility that oxidation of PDZ45 can also disrupt the INAD/PLCβ complex.

In Vivo Analysis of *inaD^{T669A}* Mutant Flies

To test the pH-dependent formation of the H-bond between T669 and H547 in vivo, we introduced the T669A mutation into full-length INAD cDNA and expressed the construct in *inaD^1* null mutant flies (*inaD^{T669A}*, Figure S7A). In wild-type photoreceptors macroscopic responses to brief flashes of light have a time-to-peak (t-pk) of ~40–50 ms, before relaxing rapidly to baseline. Responses in *inaD^{T669A}* had a similar peak amplitude but a significantly delayed t-pk (approximately 60 ms) and slightly slower decay time course (Figures 7A and 7B). Analysis of elementary responses to single photons (quantum bumps) revealed that this was primarily a consequence of a significant increase in quantum bump latency Figure S7). This would be consistent with the TRP channel and/or PLC being maintained in a low sensitivity state, resulting in delayed activation.

Following each quantum bump, believed to be generated within a single microvillus, the affected microvillus becomes flooded with Ca^{2+} and is briefly (~100 ms) refractory to further stimulation (Scott et al., 1997; Mishra et al., 2007; Liu et al., 2008). With sufficiently bright steps of illumination, this results in responses consisting of an initial peak that rapidly declines to minimum ("notch") as photons arrive in the same microvilli during the refractory period, before rebounding to a maintained plateau (Figures 7C–7E). *inad^{C645S}* mutants, in which PDZ45 should be locked in the reduced state, were previously reported to lack this "notch" suggesting that the redox switch played an important role in rendering the channels refractory during this transient period of high Ca^{2+} influx (Mishra et al., 2007). We predicted that the *inaD^{T669A}* mutation, which should lock PDZ45 in the uncoupled oxidized state, might have a converse effect. To test this we recorded responses to 1 s light steps of increasing intensity, accurately calibrated in each cell in terms of effectively absorbed photons. The intensity dependence of both peak and plateau responses in *inaD^{T669A}* were indistinguishable from controls (Figure 7F). However, consistent with a reduced sensitivity of the INAD-channel complex, when the depth of the notch in *inaD^{T669A}* was plotted against intensity (Figure 7G), it developed at significantly (approximately 2- to 3-fold) lower intensities than in controls.
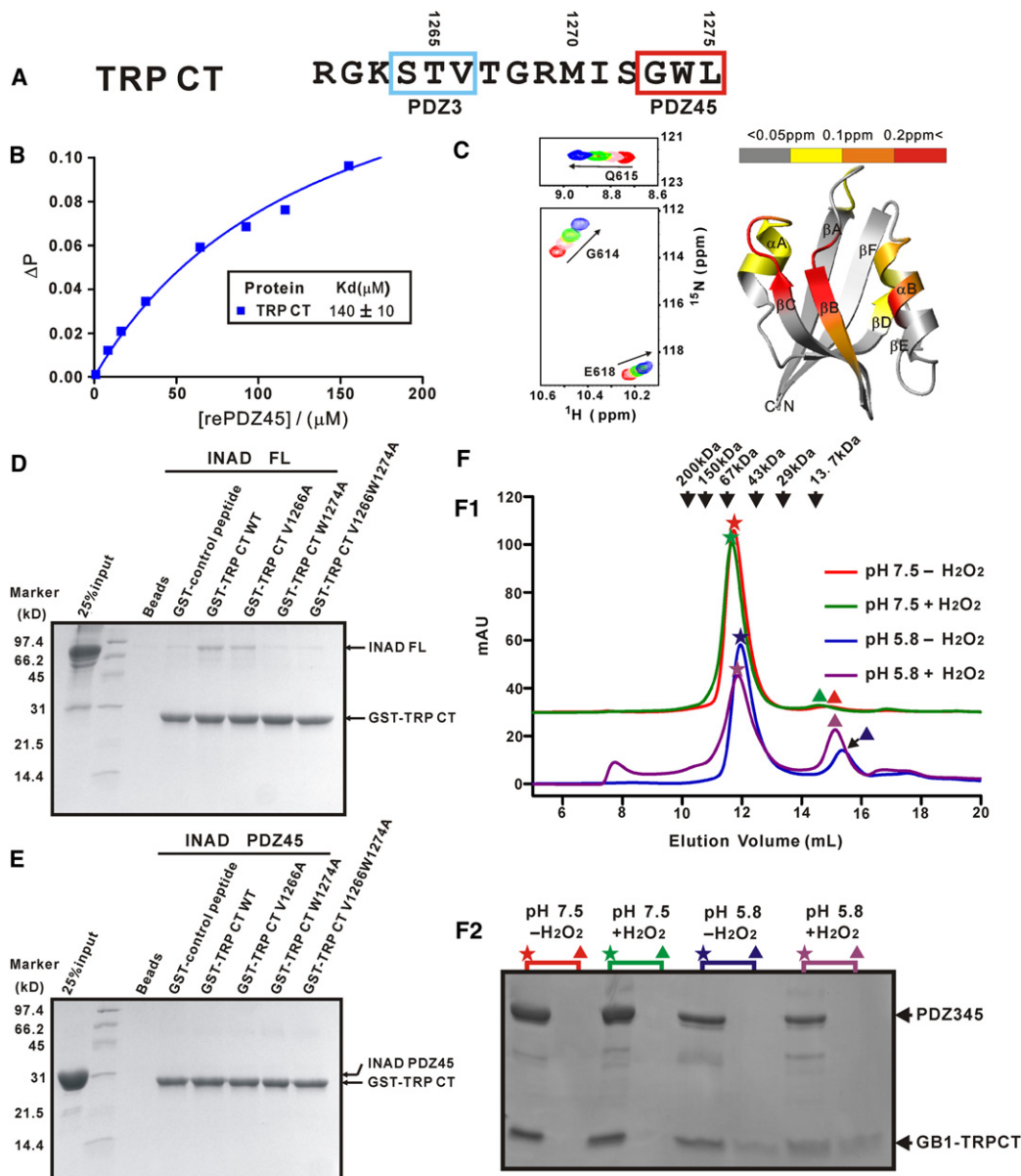
Figure 6. The Bidentate Interaction Mode between the TRP Channel and INAD

(A) Amino acid sequence of the TRP C-terminal tail. The figure depicts the internal "STV" motif as well as the "GWL" motif at the extreme end of the channel that bind to PDZ3 and PDZ45, respectively.

(B) Fluorescence-based assay showing the weak binding between the C-terminal tail TRP peptide and the INAD PDZ45 tandem.

(C) NMR chemical shift perturbation-based assay showing that the TRP peptide binds to the same pocket as the Kon peptide does. The figure also includes two selected regions of the PDZ5 HSQC spectra with the addition of increasing concentrations of the TRP peptide.

(D) In vitro pull-down assay showing that the WT GST-fused TRP C-terminal tail (15 residues) specifically binds to the full-length INAD. We used a peptide with the same length but with an irrelevant sequence to the TRP C-terminal as the binding control.

(E) The GST-fused TRP tail showed no detectable binding to PDZ45, demonstrating the essential role of the PDZ3 domain for the formation of the stable TRP/INAD complex.

(F) The INAD PDZ345/TRPCT complex undergoes a pH-dependent, oxidation-induced dissociation. Analytical gel filtration analysis showed that the purified INAD PDZ345/GB1-TRPCT complex was highly stable at pH 7.5 even when the sample was treated with 88 mM of H_2O_2 for 60 min prior to the chromatography analysis. In contrast, the PDZ345/GB1-TRPCT complex showed some degree of dissociation when the pH of the sample buffer was lowered to 5.8. Treatment of the complex in the pH 5.8 sample buffer with 88 mM of H_2O_2 for 60 min further enhanced the complex dissociation. The elution peaks corresponding to the PDZ345/TRPCT complex and the dissociated GB1-TRPCT are indicated with a star and a triangle, respectively, for each elution profile. The protein compositions of the peaks labeled were analyzed by SDS-PAGE with Coomassie blue staining and are shown in the lower panel. The elution volumes of molecular mass standards are indicated at the top of the upper panel.

Also see Figure S6.
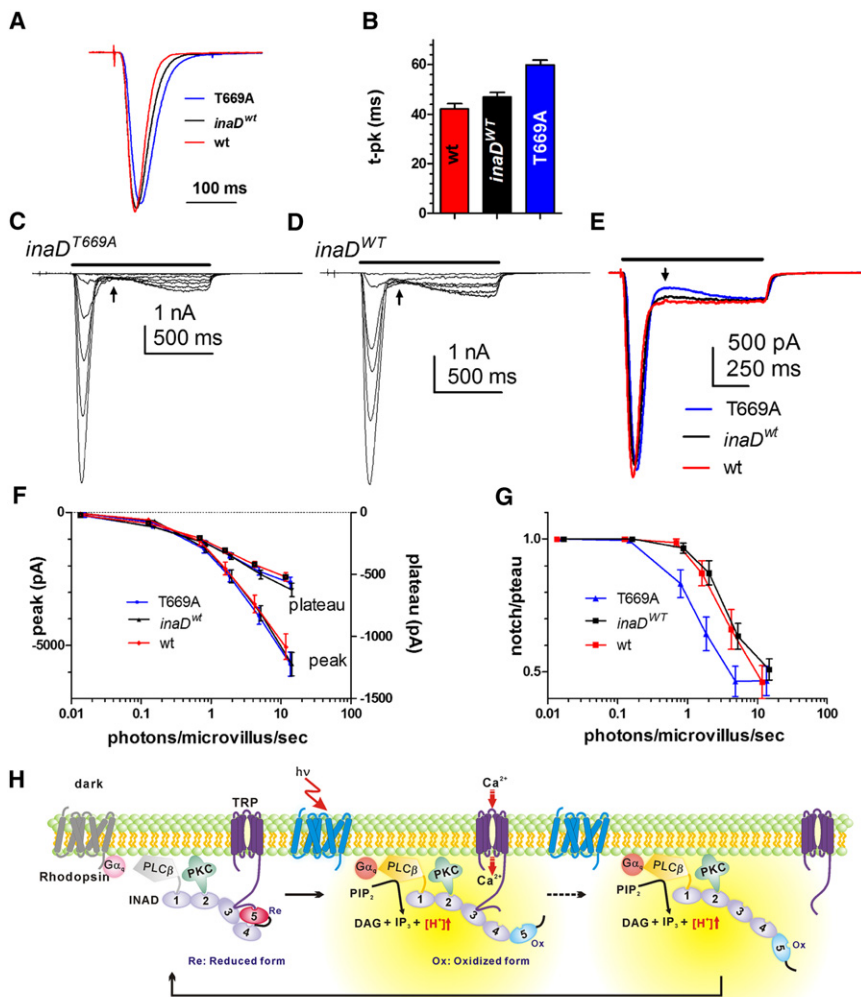
Figure 7. Whole-Cell Voltage Clamped Responses from *inaD^T669A* Mutant Photoreceptors

(A) Averaged, normalized responses to brief (1 ms) flashes containing ~75 effectively absorbed photons in photoreceptors from flies expressing *inaD^T669A* on *inaD^1* null background, wild-type (WT) and controls expressing the wild-type *inaD* transgene on an *inaD^1* null background (*inaD^WT*). Responses in *inaD^T669A* were slower that in controls.

(B) Time-to-peak (t-pk) was significantly (p < 0.01) delayed in *inaD^T669A* (mean ± standard error of the mean [SEM], n = 32 cells from two independent transformant lines).

(C and D) Responses to 1 s steps of increasing intensity (from ~400 to ~4 × 10^5 effectively absorbed photons s^-1) in *inaD^T669A* (C) and *inaD^WT* (D). Note transition from peak to plateau with marked undershoot (notch) at higher intensities (indicated by an arrow).

(E) Averaged responses from *inaD^T669A* (n = 11), *inaD^WT* (n = 7) and wild-type flies (n = 5) to a 1 s flash of effective intensity 60,000 photons. Note the pronounced notch only seen in *inaD^T669A* flies at this intensity (equivalent to ~2 photons per microvillus per second).

(F) Intensity response functions for peak response and plateau (averaged during final 100 ms of the 1 s response) for *inaD^T669A* (mean ± SEM n = 18), *inaD^WT* (n = 18), and WT (n = 10) were indistinguishable.

(G) Intensity dependence of the notch (minimum value) expressed as a fraction of the plateau level. The notch develops at ~2- to 3-fold lower intensities in *inaD^T669A* compared to controls. Error bars show mean ± SEM (n = 18). Also see Figure S7.

(H) A summary model showing the dynamic scaffolding and regulation of the INAD-organized signaling complex underneath rhabdomere membranes. In the dark, INAD adopts reduced state, and therefore the INAD complex is stoichiometrically associated with the TRP channels. In this state, the entire signaling complex is at its highest sensitivity. The light-induced increase of H+ within microvilli causes PDZ5 oxidation and TRP tail dissociation and subsequent complete dissociation of TRP from INAD PDZ345 (indicated by the dashed arrow). The dissociation of the INAD complex from the TRP channel renders the channel less sensitive, promoting its deactivation and also inducing a refractory period. INAD can quickly reassociate with the TRP channels when INAD PDZ5 return to its reduced state upon [H+] gradient dissipation, a mechanism that would promote the fast resetting of the visual signaling cycles. The *inaD^T669A* mutation locks PDZ5 in the low-affinity, oxidized state, resulting in delayed channel activation (increased bump latency). For simplicity, we have not included other regulatory elements (e.g., the feedback and feedforward regulations by Ca^2+, PKC, or PIP_2/DAG and H+-mediated regulation of the TRP channel; see (Huang et al., 2010; Yau and Hardie, 2009).

DISCUSSION

Allosteric Regulation of INAD PDZ45 Conformational Dynamics

Scaffold proteins are traditionally viewed as passive molecular adaptors that "glue" signaling proteins together. Emerging evidence indicates that, in addition to such a passive role, scaffold proteins can actively participate in dynamic regulation of signaling events (Bhattacharyya et al., 2006; Feng and Zhang, 2009). The cycling of INAD PDZ5 between the reduced and oxidized states is an elegant example of direct signaling regulation by a scaffold protein (Mishra et al., 2007), although the underlying molecular mechanism has been unclear. In this work, we discovered that the redox potential of the Cys606&645 pair of INAD PDZ5

undergoes a massive, conformation-coupled shift. Formation of the PDZ45 supramodule elevates the redox potential of PDZ5 disulfide to ~−40 mV, locking the domain in its reduced conformation capable of binding to its targets with high affinity. Conformational uncoupling between PDZ4&5 via protonation of His547 lowers the redox potential of PDZ5 to ~−370 mV, leading to the oxidation of the Cys606-Cys645 pair and consequent dissociation of PDZ5 target. Presumably, rapid dissipation of the proton gradient will restore the INAD-PDZ45 supramodule for another round of signaling event (Figure 7H).

In line with our in vitro analysis, *inaD^T669A* mutant flies, in which PDZ5 is decoupled from PDZ4 and effectively locked in the oxidized low-affinity state, display electrophysiological defects (Figure 7). Although subtle, it is striking that the defects in

inaD[T669A] were essentially the converse of those previously reported in *inaD[C645S]* mutants, where PDZ5 is locked in the reduced, high-affinity state (Mishra et al., 2007). Namely, although responses to intense flashes in *inaD[C645S]* failed to develop the "notch" characteristic of wild-type responses, the notch in *inaD[T669A]* was significantly more pronounced (Figure 7). This supports Mishra et al.'s (2007) proposal that the dynamic switch to the oxidized state is required to induce the refractory period (Hardie and Raghu 2001; Pumir et al., 2008), whereby a second photon absorbed in the same microvillus within ~100 ms fails to generate a response.

In the present study, we found that the TRP C-terminal binds avidly to the reduced PDZ345, whereas the PLC C-terminal binds with reasonably high affinity to PDZ45. Furthermore, protonation, leading to decoupling and oxidation of PDZ5, promotes dissociation of both TRP and PLC. We hypothesize that high-affinity binding of TRP and/or PLC maximizes sensitivity of the channel to activation by PLC, and that dissociation following oxidation results in a low sensitivity state (Figure 7H). In *inad[T669A]*, PDZ5 is locked in the low-affinity, low-sensitivity state, potentially accounting for both the prolonged latency and the more pronounced notch. Conversely, the notch is abolished in *inad[C654S]* mutants where PDZ45 is locked in the high-affinity, maximally sensitive state.

How might the dynamic interaction of TRP (and/or PLC) with INAD influence channel activity? TRP channels are activated by products of PIP_2 hydrolysis (putatively protons and PIP_2 depletion) and are also subject to pronounced positive and negative feedback by Ca^{2+} influx (Huang et al., 2010; for review, see Hardie and Postma, 2008). In principle, TRP's interaction with INAD could modulate the dependency of channel gating on any of these factors. It may also be relevant that PLC is dynamically regulated during phototransduction in a Ca^{2+}- and PKC-dependent manner (Gu et al., 2005).

It is noted that the oxidation speed of the Cys606&645 pair is too slow to match the extremely fast fly vision signaling kinetics. This implies that additional regulatory factor(s) must exist to regulate the fly visual signaling process. One such factor might be ePKC. It is possible that PIP_2 hydrolysis-induced acidification (via PLCβ) and INAD phosphorylation (via ePKC) act synergistically to achieve a rapid oxidation of PDZ5 required for fly visual signaling. The redox state of INAD might also be modulated by oxidants acutely generated upon light activation of fly photoreceptors, although these have not been reported to date. Alternatively, a pair of Cys with a redox potential between those of the two INAD PDZ5 conformers may function as a "facilitator" to catalyze the PDZ5 conformational cycling.

Proton as a General Second Messenger in PLC/PIP_2 Signaling Processes

It is seldom recognized that PLC-mediated hydrolysis of PIP_2 releases protons. Along with the recent finding that the light-sensitive channels in *Drosophila* can be activated by a combination of protons and phosphoinositide depletion (Huang et al., 2010), our results suggest that localized proton release by PLC may play a general role in receptor-mediated signaling processes. Proton-regulated dynamic signaling complex organization by scaffold proteins beneath PLC-containing membranes is likely to have broad implications for future studies and may force re-evaluation of many well-documented signaling events in biology.

Supramodular Nature of the INAD PDZ45 Tandem

The capacity of dynamic cycling of PDZ5 between its two distinct conformational states is enabled by the formation of the PDZ45 supramodule. The INAD PDZ45 supramodule, together with a number of recent examples, demonstrates that two or more PDZ domains connected in tandem often display distinct target-binding properties from each isolated domain or the simple sum of the isolated PDZ domains due to direct interactions of PDZ domains in the tandem (Feng et al., 2003; Long et al., 2003, 2005, 2008). An additional advantage of arranging multiple protein modules into a higher order supramodule is to build regulatory mechanisms into scaffold proteins, thereby enabling them to actively control signaling events organized around them (Feng and Zhang, 2009). INAD takes the supramodule feature to another level. Productive binding between TRP channel and INAD requires PDZ3 and PDZ45 to be covalently linked together forming a PDZ345 supramodule.

Conformation-Coupled Modulation of Protein Disulfide Redox Potentials

Cys oxidations are known to regulate very broad cellular activities. It is generally accepted that oxidations of Cys in proteins occur either via a limited degree of cellular redox potential changes or generations of reactive oxidants as a result of cellular metabolism/signaling (Janssen-Heininger et al., 2008; Rhee, 2006). In this paradigm, Cys residues in proteins act as sensors by passively responding to cellular redox potential changes or generations of reactive oxygen species, as redox potentials of protein disulfides generally do not change. Formation of inter- or intramolecular disulfide bonds are increasingly recognized as important activity regulatory mechanisms for cellular proteins and enzymes (see Ago et al., 2008; Fox et al., 2007; Kemble and Sun, 2009 for examples). The disulfide-mediated oxidation of INAD PDZ45 characterized in this work represents an unprecedented protein oxidation mechanism. The redox potential of the disulfide bond in PDZ5 is allosterically regulated by the conformational coupling of PDZ4. Formation of the PDZ45 supramodule raise the standard redox potential of PDZ5 by as much as 330 mV, thereby converting the Cys606-Cys645 disulfide of PDZ5 from the highly stable oxidized state to the extremely stable reduced state at cellular redox potentials. In view of the widespread existence of Cys residues in cellular proteins and enzymes, it is possible that such conformation-dependent redox potential oscillations also exist in other proteins. Such regulated, large amplitude redox potential oscillations of proteins and enzymes may be a general paradigm for cellular signal transduction regulations. One may envision that a combined action of reactive oxygen species and redox potential oscillations can further sharpen redox signaling events spatiotemporally.

EXPERIMENTAL PROCEDURES

Protein Expression and Purification
Drosophila PDZ5 and PDZ45 were expressed in and purified in bacteria (see Extended Experimental Procedures for details).

Fluorescence Assay

Fluorescence assays were performed on a PerkinElmer LS-55 fluorimeter at 20°C. In the assay, FITC (Molecular Probes) labeled peptide samples (∼1 μM) were titrated with binding partners in buffer containing 50 mM Tris (with pH value and DTT concentration specifically indicated, 50 mM NaCl, and 1 mM EDTA), and the titration curves were fitted with the GraphPad Prism 5 software package.

Redox Measurements of PDZ5 and PDZ45

Redox kinetics and thermodynamics (i.e., the standard redox potentials) of PDZ5 and PDZ45 were measured by NMR spectroscopy and the Ellman chemistry. Detailed procedures can be found in Extended Experimental Procedures.

NMR Structure Determination

All protein samples used for NMR titration experiments were concentrated to 0.2∼0.5 mM in 50 mM Tris (pH 7.0, with 1 mM EDTA and 50 mM NaCl, with DTT concentrations specified). NMR spectra were acquired at 30°C on Varian NMR spectrometers. The PDZ5/Kon peptide complex was determined using standard NMR methods (see Extended Experimental Procedures for details).

Crystallography

Crystals of the PDZ45/NG2 peptide complex and the Se-Met-labeled PDZ45/NG2 peptide complex were obtained by the hanging drop vapor diffusion method at 16°C. The PDZ45/NG2 peptide complex crystals grew in the crystallization buffer containing 2.4 M $(NH_4)_2SO_4$, and 0.1 M Tris (pH 8.5). The native and Se-Met X-ray data sets were collected at the Cornell High-Energy Synchrotron Source beamline A1. The detailed X-ray crystallographic methods can be found in the Extended Experimental Procedures.

GST Pull-Down Assay

In vitro binding between TRP C-terminal tail and INAD was assayed using GSH-Sepharose beads-based pull-down assay. INAD proteins (140 μg for INAD FL and 50 μg for PDZ45 in each assay) were first cleared by preincubating with 30 μl of GSH-Sepharose beads in 1 ml assay buffer (50 mM Tris-HCl [pH 7.5] containing 1 M NaCl, 1 mM DTT). Precleared INAD proteins were then mixed with 30 μl of GSH-Sepharose beads charged with 20 μg GST-TRP-CT at 4°C for 30 min. The GSH-Sepharose beads were washed three times with the assay buffer, and the retained proteins were assayed by SDS-PAGE with Coomassie blue staining.

Analytical Gel Filtration Chromatography

Analytical gel filtration chromatography was carried out on an AKTA FPLC system (GE Healthcare). Proteins were loaded on to a Superose 12 10/300 GL column 20 (GE Healthcare) equilibrated with a buffer containing 50 mM Tris-HCl (pH 7.5, with 100 mM NaCl, and 1 mM EDTA with or without 1 mM DTT).

Flies

Drosophila melanogaster were raised in the dark at 25°C. The wild-type strain was w^{1118}. Transgenic lines expressing $inaD^{T669A}$ and $inaD^{WT}$ cDNA under the Rh1 promoter were generated by standard P-element transformation and recombined into a $inaD^1$ null background (Tsunoda et al., 1997).

Electrophysiology

Dissociated ommatidia were prepared as previously described (e.g., Henderson et al., 2000; Hardie et al., 2002) from newly eclosed adult flies and transferred to a recording chamber on an inverted Nikon Diaphot microscope. Whole-cell voltage clamp recordings were made at room temperature (20°C ± 1°C) at −70 mV using electrodes of resistance ∼10–15 MΩ using standard solutions (see Extended Experimental Procedures for further details). Photoreceptors were stimulated via a green light-emitting diode; intensities were calibrated in every cell in terms of effectively absorbed photons by counting quantum bumps at low intensities.

ACCESSION NUMBERS

The coordinates of the PDZ5/Kon and PDZ45/NG2 complexes have been deposited in the Protein Data Bank under the accession codes of 2LA8 and 3R0H, respectively.

SUPPLEMENTAL INFORMATION

Supplemental Information includes Extended Experimental Procedures, seven figures, and two tables and can be found with this article online at doi:10.1016/j.cell.2011.05.015.

REFERENCES

Adamski, F.M., Zhu, M.Y., Bahiraei, F., and Shieh, B.H. (1998). Interaction of eye protein kinase C and INAD in Drosophila. Localization of binding domains and electrophysiological characterization of a loss of association in transgenic flies. J. Biol. Chem. *273*, 17713–17719.

Ago, T., Liu, T., Zhai, P., Chen, W., Li, H., Molkentin, J.D., Vatner, S.F., and Sadoshima, J. (2008). A redox-dependent pathway for regulating class II HDACs and cardiac hypertrophy. Cell *133*, 978–993.

Bhattacharyya, R.P., Remenyi, A., Yeh, B.J., and Lim, W.A. (2006). Domains, motifs, and scaffolds: the role of modular interactions in the evolution and wiring of cell signaling circuits. Annu. Rev. Biochem. *75*, 655–680.

Chevesich, J., Kreuz, A.J., and Montell, C. (1997). Requirement for the PDZ domain protein, INAD, for localization of the TRP store-operated channel to a signaling complex. Neuron *18*, 95–105.

Feng, W., and Zhang, M. (2009). Organization and dynamics of PDZ-domain-related supramodules in the postsynaptic density. Nat. Rev. Neurosci. *10*, 87–99.

Feng, W., Shi, Y., Li, M., and Zhang, M. (2003). Tandem PDZ repeats in glutamate receptor-interacting proteins have a novel mode of PDZ domain-mediated target binding. Nat. Struct. Biol. *10*, 972–978.

Fox, G.C., Shafiq, M., Briggs, D.C., Knowles, P.P., Collister, M., Didmon, M.J., Makrantoni, V., Dickinson, R.J., Hanrahan, S., Totty, N., et al. (2007). Redox-mediated substrate recognition by Sdp1 defines a new group of tyrosine phosphatases. Nature *447*, 487–492.

Gu, Y., Oberwinkler, J., Postma, M., and Hardie, R.C. (2005). Mechanisms of light adaptation in Drosophila photoreceptors. Curr. Biol. *15*, 1228–1234.

Hardie, R.C., and Raghu, P. (2001). Visual transduction in *Drosophila*. Nature *413*, 186–193.

Hardie, R.C., and Postma, M. (2008). Phototransduction in microvillar photoreceptors of Drosophila and other invertebrates. In The Senses-a comprehensive reference Vision, *Volume 1*, T.D. Albright and R. Masland, eds. (Oxford: Academic Press), pp. 77–130.

Hardie, R.C., Peretz, A., Suss-Toby, E., Rom-Glas, A., Bishop, S.A., Selinger, Z., and Minke, B. (1993). Protein kinase C is required for light adaptation in *Drosophila* photoreceptors. Nature *363*, 634–637.

Hardie, R.C., Martin, F., Cochrane, G.W., Juusola, M., Georgiev, P., and Raghu, P. (2002). Molecular basis of amplification in *Drosophila* phototransduction. Roles for G protein, phospholipase C, and diacylglycerol kinase. Neuron *36*, 689–701.

Henderson, S.R., Reuss, H., and Hardie, R.C. (2000). Single photon responses in Drosophila photoreceptors and their regulation by Ca2+. J. Physiol. *524*, 179–194.

Huang, J., Liu, C.H., Hughes, S.A., Postma, M., Schwiening, C.J., and Hardie, R.C. (2010). Activation of TRP channels by protons and phosphoinositide depletion in Drosophila photoreceptors. Curr. Biol. *20*, 189–197.

Huber, A. (2001). Scaffolding proteins organize multimolecular protein complexes for sensory signal transduction. Eur. J. Neurosci. *14*, 769–776.

Huber, A., Sander, P., Gobert, A., Bahner, M., Hermann, R., and Paulsen, R. (1996a). The transient receptor potential protein (Trp), a putative store-operated Ca2+ channel essential for phosphoinositide-mediated photoreception, forms a signaling complex with NorpA, InaC and InaD. EMBO J. *15*, 7036–7045.

Huber, A., Sander, P., and Paulsen, R. (1996b). Phosphorylation of the InaD gene product, a photoreceptor membrane protein required for recovery of visual excitation. J. Biol. Chem. *271*, 11710–11717.

Janssen-Heininger, Y.M.W., Mossman, B.T., Heintz, N.H., Forman, H.J., Kalyanaraman, B., Finkel, T., Stamler, J.S., Rhee, S.G., and van der Vliet, A. (2008). Redox-based regulation of signal transduction: Principles, pitfalls, and promises. Free Radic. Biol. Med. *45*, 1–17.

Juusola, M., and Hardie, R.C. (2001). Light adaptation in Drosophila photoreceptors: I. Response dynamics and signaling efficiency at 25 degrees C. J. Gen. Physiol. *117*, 3–25.

Keese, M.A., Saffrich, R., Dandekar, T., Becker, K., and Schirmer, R.H. (1999). Microinjected glutathione reductase crystals as indicators of the redox status in living cells. FEBS Lett. *447*, 135–138.

Kemble, D.J., and Sun, G. (2009). Direct and specific inactivation of protein tyrosine kinases in the Src and FGFR families by reversible cysteine oxidation. Proc. Natl. Acad. Sci. USA *106*, 5070–5075.

Kimple, M.E., Siderovski, D.P., and Sondek, J. (2001). Functional relevance of the disulfide-linked complex of the N-terminal PDZ domain of InaD with NorpA. EMBO J. *20*, 4414–4422.

Li, H.S., and Montell, C. (2000). TRP and the PDZ protein, INAD, form the core complex required for retention of the signalplex in Drosophila photoreceptor cells. J. Cell Biol. *150*, 1411–1422.

Liu, C.H., Satoh, A.K., Postma, M., Huang, J., Ready, D.F., and Hardie, R.C. (2008). Ca^{2+}-dependent metarhodopsin inactivation mediated by calmodulin and NINAC myosin III. Neuron *59*, 778–789.

Long, J., Wei, Z., Feng, W., Yu, C., Zhao, Y.X., and Zhang, M. (2008). Supramodular nature of GRIP1 revealed by the structure of its PDZ12 tandem in complex with the carboxyl tail of Fras1. J. Mol. Biol. *375*, 1457–1468.

Long, J.F., Tochio, H., Wang, P., Fan, J.S., Sala, C., Niethammer, M., Sheng, M., and Zhang, M. (2003). Supramodular structure and synergistic target binding of the N-terminal tandem PDZ domains of PSD-95. J. Mol. Biol. *327*, 203–214.

Long, J.F., Feng, W., Wang, R., Chan, L.N., Ip, F.C., Xia, J., Ip, N.Y., and Zhang, M. (2005). Autoinhibition of X11/Mint scaffold proteins revealed by the closed conformation of the PDZ tandem. Nat. Struct. Mol. Biol. *12*, 722–728.

Mishra, P., Socolich, M., Wall, M.A., Graves, J., Wang, Z., and Ranganathan, R. (2007). Dynamic scaffolding in a G protein-coupled signaling system. Cell *131*, 80–92.

Montell, C. (1999). Visual transduction in Drosophila. Annu. Rev. Cell Dev. Biol. *15*, 231–268.

Montell, C. (2003). The venerable inveterate invertebrate TRP channels. Cell Calcium *33*, 409–417.

Montell, C. (2005). TRP channels in Drosophila photoreceptor cells. J. Physiol. *567*, 45–51.

Ostergaard, H., Tachibana, C., and Winther, J.R. (2004). Monitoring disulfide bond formation in the eukaryotic cytosol. J. Cell Biol. *166*, 337–345.

Pawson, T., and Nash, P. (2003). Assembly of cell regulatory systems through protein interaction domains. Science *300*, 445–452.

Peng, L., Popescu, D.C., Wang, N., and Shieh, B.H. (2008). Anchoring TRP to the INAD macromolecular complex requires the last 14 residues in its carboxyl terminus. J. Neurochem. *104*, 1526–1535.

Popescu, D.C., Ham, A.J., and Shieh, B.H. (2006). Scaffolding protein INAD regulates deactivation of vision by promoting phosphorylation of transient receptor potential by eye protein kinase C in Drosophila. J. Neurosci. *26*, 8570–8577.

Pumir, A., Graves, J., Ranganathan, R., and Shraiman, B.I. (2008). Systems analysis of the single photon response in invertebrate photoreceptors. Proc. Natl. Acad. Sci. USA *105*, 10354–10359.

Rhee, S.G. (2006). Cell signaling. H2O2, a necessary evil for cell signaling. Science *312*, 1882–1883.

Schafer, F.Q., and Buettner, G.R. (2001). Redox environment of the cell as viewed through the redox state of the glutathione disulfide/glutathione couple. Free Radic. Biol. Med. *30*, 1191–1212.

Scott, K., Sun, Y., Beckingham, K., and Zuker, C.S. (1997). Calmodulin regulation of Drosophila light-activated channels and receptor function mediates termination of the light response in vivo. Cell *91*, 375–383.

Shieh, B.H., and Zhu, M.Y. (1996). Regulation of the TRP Ca2+ channel by INAD in Drosophila photoreceptors. Neuron *16*, 991–998.

Smith, D.P., Ranganathan, R., Hardy, R.W., Marx, J., Tsuchida, T., and Zuker, C.S. (1991). Photoreceptor deactivation and retinal degeneration mediated by a photoreceptor-specific protein kinase C. Science *254*, 1478–1484.

Tsunoda, S., and Zuker, C.S. (1999). The organization of INAD-signaling complexes by a multivalent PDZ domain protein in Drosophila photoreceptor cells ensures sensitivity and speed of signaling. Cell Calcium *26*, 165–171.

Tsunoda, S., Sierralta, J., Sun, Y., Bodner, R., Suzuki, E., Becker, A., Socolich, M., and Zuker, C.S. (1997). A multivalent PDZ-domain protein assembles signalling complexes in a G-protein-coupled cascade. Nature *388*, 243–249.

van Huizen, R., Miller, K., Chen, D.M., Li, Y., Lai, Z.C., Raab, R.W., Stark, W.S., Shortridge, R.D., and Li, M. (1998). Two distantly positioned PDZ domains mediate multivalent INAD-phospholipase C interactions essential for G protein-coupled signaling. EMBO J. *17*, 2285–2297.

Wang, T., and Montell, C. (2007). Phototransduction and retinal degeneration in Drosophila. Pflugers Arch. *454*, 821–847.

Xu, X.Z., Choudhury, A., Li, X., and Montell, C. (1998). Coordination of an array of signaling proteins through homo- and heteromeric interactions between PDZ domains and target proteins. J. Cell Biol. *142*, 545–555.

Yau, K.W., and Hardie, R.C. (2009). Phototransduction motifs and variations. Cell *139*, 246–264.

Zhang, M., and Wang, W. (2003). Organization of signaling complexes by PDZ-domain scaffold proteins. Acc. Chem. Res. *36*, 530–538.